Phi: Jurnal Pendidikan Fisika dan Terapan
Vol. 12, No. 2 (2026) 344-355
ISSN: 2460-4348, e-ISSN: 2549-7162
https://jurnal.ar-raniry.ac.id/index.php/jurnalphi/index

Article Type: *original research*

Identification of Coal Seams Using Ground Penetrating Radar (GPR) Integrated with Borehole Logging Data at PIT "SWIM", South Palembang Sub-Basin

Vivin Julianty Situmorang[1*], Andri Yadi Paembonan[1], Putu Pradnya Andika[1], Muhammad Alamshah[2]

[1]Department of Geophysical Engineering, Faculty of Industrial Technology, Sumatera Institute of Technology, South Lampung

[2]PT Bukit Asam (Persero) Tbk, Tanjung Enim

Correspondence E-mail: vivinsitumorang23@gmail.com

ARTICLE INFO

Article History:
Received: 22 April 2026
Revised: 26 June 2026
Accepted: 14 July 2026
Published: 19 July 2026

Keywords:
Ground penetrating radar; Coal; Electromagnetic; Dielectric constant; Amplitude.

ABSTRACT

Coal remains one of the main energy sources in Indonesia, contributing more than 40% to national energy consumption. Therefore, an effective exploration method is needed to identify subsurface coal seams. This study aims to identify the presence of coal seams using the Ground Penetrating Radar (GPR) method integrated with borehole logging data at PIT "SWIM", South Palembang Sub-Basin. The study utilized four GPR survey lines and four borehole log datasets. The GPR data were acquired using a 25 MHz antenna frequency and processed through the stages of move starttime, dewow filtering, automatic gain control, bandpass Butterworth filtering, background removal, running average, and topography correction Interpretation was carried out based on reflection patterns, reflector continuity, amplitude characteristics, and correlation with gamma-ray and density logs. The results indicate five coal seam zones, namely A1, A2, B, C, and D, at depths of approximately 8–60 m. Among these, Seam B exhibits the most consistent continuity across the survey lines, while Seam D appears as a prominent deeper reflector. Strong, continuous, high-amplitude reflectors indicate significant dielectric property contrasts between the coal and the surrounding lithologies. This study demonstrates that the integration of low-frequency (25 MHz) GPR and logging data can effectively support coal seam identification and illustrates the application of electromagnetic wave propagation, reflection, attenuation, and dielectric contrast principles in subsurface exploration, making it relevant to the fields of applied physics and geophysics.

This work is licensed under a Creative Commons Attribution-ShareAlike 4.0 International License

1. INTRODUCTION

Indonesia is one of the countries with very high energy consumption. This condition has led to the continued reliance on fossil energy sources as the primary choice, including coal, which to this day remains an important energy source in Indonesia for meeting national energy needs. Based on data from the Ministry of Energy and Mineral Resources of the Republic of Indonesia (2021), coal remains the dominant primary energy source in Indonesia, with coal accounting for more than 40% of the total energy supply and roughly 65-69%of electricity generation. Indonesia possesses enormous coal potential, with total resources of 143.73 billion tons and reserves of 38.80 billion tons.

Coal resources and reserves in Indonesia are generally concentrated in Sumatra and Kalimantan (Ministry of Energy and Mineral Resources, 2021). Among the distribution of these resources, the South Palembang Sub-Basin is one of the largest coal-producing regions in Indonesia, with production having increased significantly over the past 5 years. In 2025, coal production is targeted to increase to reach 147.33 million tons (South Sumatra Provincial Government, 2025). This potential can be widely utilized as an energy source, particularly for power generation.

The geological conditions of the study area, located in the South Palembang Sub-Basin, originated from sedimentary depositional processes during the Tertiary period and were influenced by tectonic activity associated with the subduction of the Indo-Australian Plate, resulting in a non-uniform distribution of coal seams (Barber et al., 2005; Ramadhana et al., 2022). The study area, situated within the Muara Enim Formation, is one of the rock-forming units in the South Palembang Sub-Basin that was deposited in shallow marine, non-marine, and deltaic plain environments, with constituent lithologies consisting of sandstone, siltstone, claystone, and coal, with tuff or tuffaceous claystone occasionally found in the upper sections (Barber et al., 2005). This formation reflects a second regressive cycle initiated by deposition in a coastal plain swamp environment, particularly in the southern part of the South Sumatra Basin, where extensive coal deposits were produced. Subsequently, the depositional process evolved into a delta plain environment, characterized by thick shale and sandstone deposits (Anwar et al., 2021). Under these conditions, coal formation began with the deposition of organic plant material in the basin, which then underwent decomposition influenced by factors such as temperature, water circulation, and acidity (Jovanovski et al., 2023). The product of this peatification process subsequently underwent compaction by the overlying layers due to excessive pressure during the coalification stage (Nursanto et al., 2023).

The exploration process commonly carried out in the area employs the well logging method, which records and identifies responses of physical rock properties by interpreting log data displayed only vertically to determine lithological boundaries, thickness, and subsurface depth (Farahdila & Setiawan, 2023). However, coal exploration also requires lateral information to determine the continuity of coal seams in support of coal mining activities (Unver, 2018). Therefore, geophysical methods, particularly Ground Penetrating Radar (GPR), are greatly needed, as they can clearly delineate the boundary between coal and the surrounding rocks through amplitude variations arising from contrasts in their physical properties, namely permittivity and conductivity (Tian et al., 2025). The relationship between the physical properties of rocks and the electromagnetic wave responses recorded on a radargram provides a direct illustration of how physics concepts are used to interpret subsurface conditions.

In its application to coal exploration, the GPR method can identify coal seams based on wave reflection characteristics, velocity, and differences in properties such as the dielectric constant between layers. Previous studies conducted in the same formation have shown that GPR can identify the continuity of coal seams through radargram interpretation and velocity analysis (Jufri et al., 2015). The GPR method is also capable of mapping the geometry and thickness of coal seams laterally (Ibrahim et al., 2007). However, those studies only used GPR results to identify coal seams therefore, in this study, a correlation with log data was performed to validate the actual presence of coal seams.

2. METHODS

2.1 Ground Penetrating Radar (GPR)

GPR is a method that provides a depiction of subsurface conditions by propagating high-frequency electromagnetic waves (1 MHz – 3 GHz) and utilizing their electrical and magnetic properties (Fang et al., 2023; Syukri, 2020). As the waves propagate into the ground, they encounter boundaries between layers with contrasting dielectric properties, such as differences in water content, material composition, or material density. The dielectric constant's physical properties greatly influence the velocity, attenuation, reflection, refraction, and transmission of electromagnetic waves. Reflection in GPR is influenced by the dielectric constant, conductivity, and antenna frequency. High-frequency antennas provide high resolution but shallow penetration depth, while low-frequency antennas offer lower resolution with deeper penetration (Feng et al., 2023)

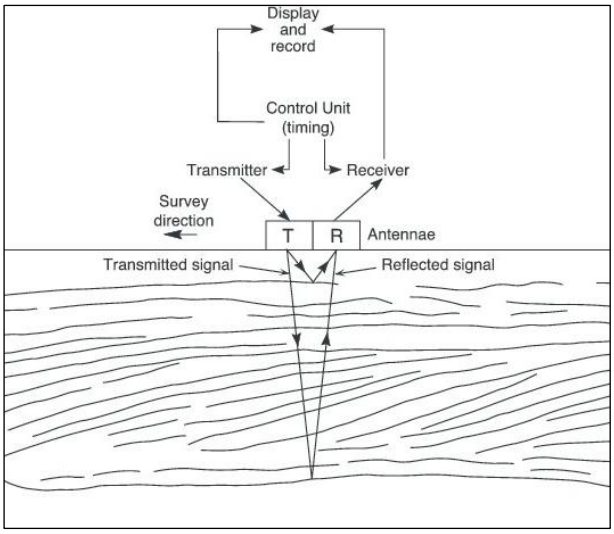


Figure 1. Working principle of Ground Penetrating Radar (GPR) (Neal, 2004)

Figure 1 shows that the main components of the GPR instrument are the transmitter, receiver, and control unit. Electromagnetic waves are emitted by the transmitter toward the subsurface. When these waves encounter an object or material with different dielectric properties beneath the surface, attenuation occurs, causing the received signal to reflect the differences in dielectric permittivity. The emitted waves can also spread over a wider area, as part of their energy is absorbed by material layers with higher dielectric permittivity. When the signal returns to the surface at varying angles or distances, the received radar reflections will exhibit variations in amplitude due to differences in subsurface material properties (Priyanka et al., 2022). Theoretically, the magnitude of the wave energy reflected at the boundary between two media can be expressed through the reflection coefficient as follows:

$$R = \frac{\sqrt{\varepsilon_2} - \sqrt{\varepsilon_1}}{\sqrt{\varepsilon_2} + \sqrt{\varepsilon_1}} \quad (1)$$

where R = reflection coefficient, ε_1= relative dielectric constant of the first layer, ε_2= relative dielectric constant of the second layer (Daniels, 2004). The value of this reflection coefficient indicates that the greater the difference in electromagnetic properties between layers, the greater the wave energy that is reflected and recorded by the GPR system.

The two-way travel time difference between the transmitted and received electromagnetic waves is the primary parameter for estimating the depth and thickness of a subsurface layer. This principle utilizes the wave propagation velocity in a given medium, so that variations in travel time can be converted into subsurface geometry information. GPR measurement data are then displayed as a radargram, which represents the wave reflection response to differences in the physical properties of materials. The reflection patterns appearing in the radargram can be interpreted as indications of lithological changes, layer boundaries, or the presence of specific objects beneath the surface (Neal, 2004).

The portion of the wave that is not reflected will continue to propagate until it reaches the next layer boundary (interface). Electromagnetic waves are field waves that propagate with a vibration direction perpendicular to their direction of propagation. In their propagation, electromagnetic waves travel through subsurface media with specific physical properties. These waves consist of two main components, namely the electric and magnetic fields, which oscillate perpendicular to each other. When propagating through subsurface geological layers, electromagnetic waves undergo various interactions, including diffraction, reflection, and transmission. These interactions are governed by the physical properties of the medium, such as magnetic permeability (μ), electrical permittivity (ε), dan conductivity (σ) (Jol, 2009).

In the propagation of electromagnetic waves, when passing through different media, amplitude attenuation occurs as depth increases due to the attenuation phenomenon, which can be mathematically expressed as:

$$\alpha = \omega\sqrt{\frac{\mu\varepsilon}{2}}\left[\left(\left(1+\frac{\sigma^2}{\omega^2\varepsilon^2}\right)^{\frac{1}{2}}-1\right)^{\frac{1}{2}}\right] \quad (2)$$

$$\alpha \approx \frac{\sigma}{2}\sqrt{\frac{\mu}{\varepsilon}}\ ;\ \sigma \ll \omega\varepsilon \quad (3)$$

As signal attenuation increases, the penetration depth of electromagnetic waves becomes limited (Balanis, 2012). This can be explained through the concept of skin depth, which indicates how deep an electromagnetic wave can penetrate a given medium, and is formulated as follows:

$$\delta \approx 0.0053\frac{\sqrt{\varepsilon_r}}{\sigma}\ ;\sigma \ll \omega\varepsilon \quad (4)$$

where $\alpha =$ attenuation constant (Np/m), $\omega =$ angular frequency (rad/s), $\delta =$ skin depth (meter), $\sigma =$ conductivity (s/m), $f =$ frequency (Hz), $\varepsilon_r =$ dielectric constant/relative permittivity. The higher the frequency used, the smaller the skin depth, resulting in shallower penetration depth but higher resolution (Jol, 2009).

2.2 Study Area and Data Processing

Based on the regional geological map shown in Figure 2, the study area is located within the Muara Enim Formation (Tmpm). This formation was developed during the regression phase of a shallow-marine–transitional–shallow-marine facies sequence. The Muara Enim Formation is composed of claystone, siltstone, and tuffaceous sandstone with intercalated coal layers.

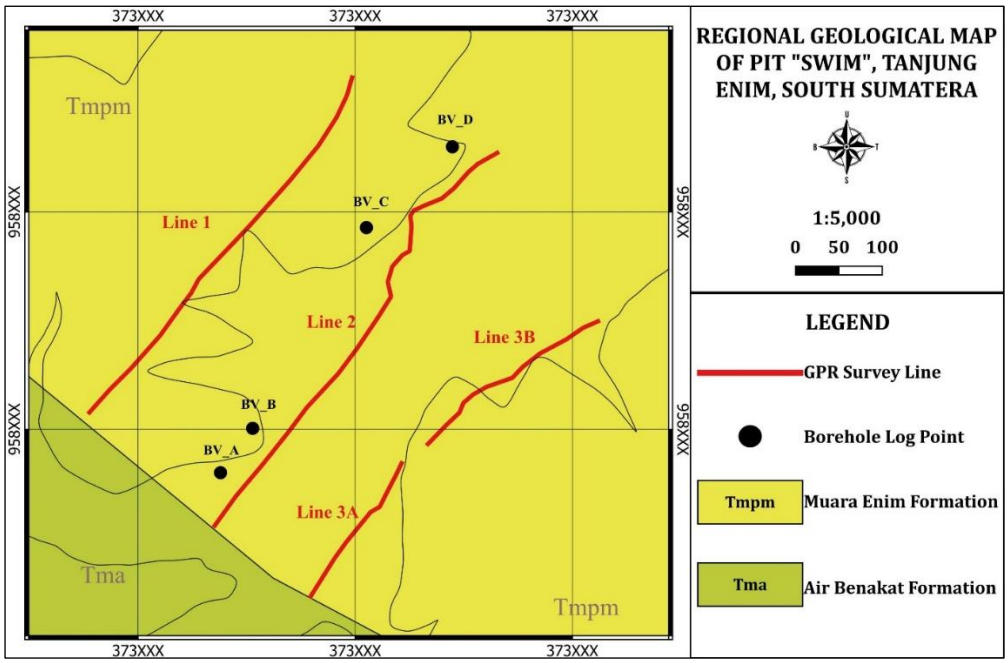


Figure 2. Regional geological map showing the 4 GPR survey lines and 4 borehole locations

The data measurements were done with a MALA Geoscience instrument from Sweden, operating at 25 MHz. This typical frequency has an effective depth range of up to 60 meters (Geo, 2023). The 25 MHz GPR antenna was selected because it has greater penetration depth, making it suitable for detecting coal seams at depths of tens of meters, although its resolution is lower than

that of higher frequencies. Interpretation was only carried out in zones that still exhibited clear reflectors and amplitudes (Francke & Utsi, 2009).

The study was conducted in the open-pit mining area of PIT "SWIM" in Tanjung Enim, South Sumatra. Data acquisition involved 4 GPR survey lines, each 500 meters (line 1), 585 meters (line 2), 191 meters (line 3A), 246 meters (line 3B), and was supported by data 4 borehole log points, as shown in Figure 2. The GPR data and log data obtained were then processed to produce clearer radargrams and vertical cross-sections for interpretation. The processing stages can be simply seen in the flowchart in Figure 3.

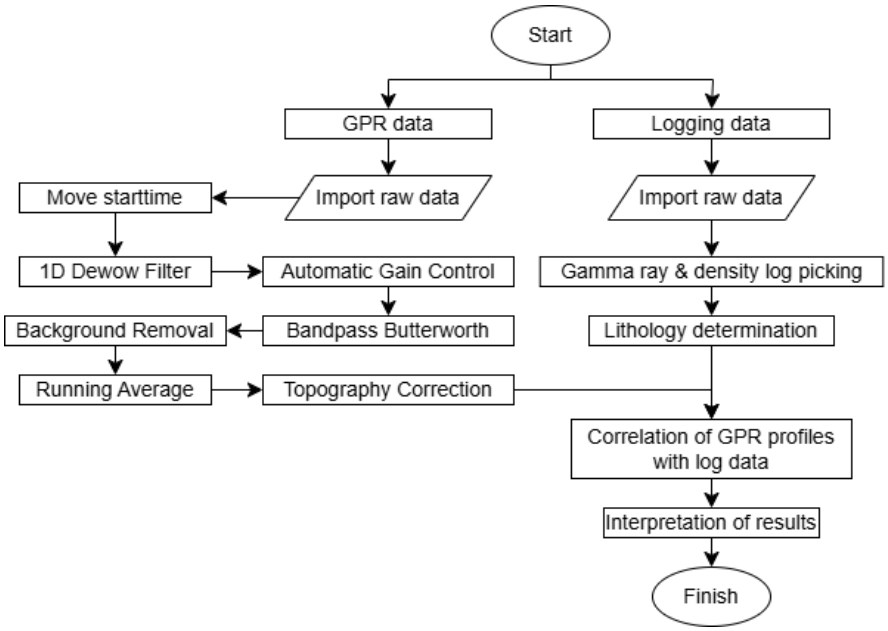


Figure 3. Research methodology flowchart

The data processing stages began with move starttime, which is the process of removing unwanted signals such as early noise, thereby resetting the first wave arrival time to 0 ns (Marbun et al., 2020), followed by subtract-mean (dewow), a filter used to remove very low-frequency noise (Marbun et al., 2020). Subsequently, automatic gain control (AGC) was applied to amplify the signal, as electromagnetic waves emitted into the subsurface become increasingly weak with depth due to attenuation (Marbun et al., 2020). This was followed by the bandpass butterworth filter, which functions to eliminate unwanted frequencies (noise) by limiting the frequency range values (Rumansah et al., 2025). Background removal was then applied to eliminate background noise that obscures the primary signal and to remove low-frequency horizontal coherent energy (Elfarabi et al., 2017), followed by running average to smooth the signal by averaging several adjacent traces in order to clarify reflection patterns (Rumansah et al., 2025), and finally topography correction to adjust the radargram results to the topographic conditions in the field at the time of measurement (Sandmeier, 2020). The GPR radargram processing parameters are presented in Table 1.

Table 1. GPR processing parameters

Tahapan Processing	Parameter
Move starttime	Move time (ns): -68.711
1D filter subtract-mean (Dewow)	Timewindow (ns): 40
Automatic Gain Control (AGC)	Window length: 20
Bandpass butterworth	Lower cutoff: 15 MHz Upper cutoff: 35 MHz
Background removal	Default setting
Running average	Average traces: 1
Topography correction	Coordinate and topography input

The processing results are displayed as radargram cross-sections showing the wave travel time on the vertical axis, which can be converted to depth using Equation 5 as follows:

$$z = \frac{v \, . \, t}{2} \tag{5}$$

where v is the electromagnetic wave velocity in the subsurface material and t is the two-way travel time of the GPR signal. In the radargram, the vertical axis represents travel time converted to depth, while the horizontal axis represents survey distance. An initial velocity range of 0.13–0.15 m/ns was adopted based on the electromagnetic wave velocity table reported by (Daniels, 2004) and previous studies conducted in the same geological setting (Ibrahim et al., 2007; Jufri et al., 2015). The velocity was subsequently calibrated through well-tie correction by matching reflector continuity on the radargram with lithological boundaries identified from borehole logs, resulting in a fixed velocity of 0.14 m/ns. The GPR interpretation was further constrained using borehole log data processed in WellCAD, where gamma-ray and density logs were analyzed to delineate lithological boundaries based on their characteristic responses.

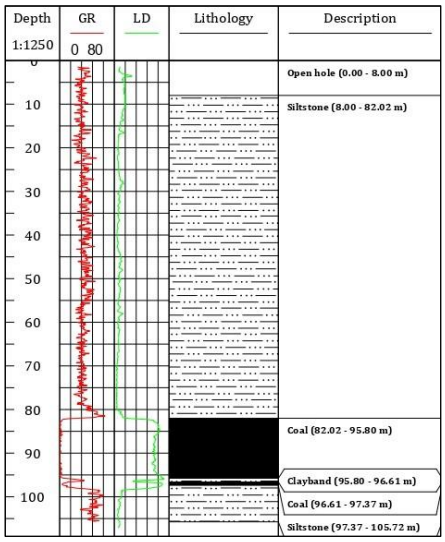
3. RESULT AND DISCUSSION

Based on the radargram results of all GPR survey lines, coal layer zones can be indicated by sharper reflection patterns compared to other reflection patterns. These patterns indicate the presence of boundaries between layers with varying physical property characteristics. This is attributed to coal's high carbon content, which influences the physical response to the emitted electromagnetic waves.

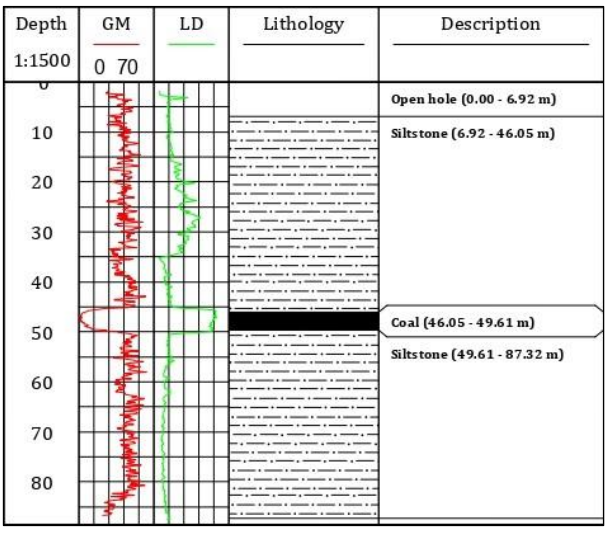
Table 2. Rock log characteristics (Adrian & Mulyatno, 2020; Alifa, 2024)

Lithology	Log Characteristics	
	Gamma Ray (API)	Density (gr/cc)
Coal	0.00 – 11.00	1.2 – 1.8
Sandstone	30 - 45	2.0 – 2.6
Siltstone	15 - 35	2.1 – 2,5
Claystone	45 - 70	2.2 – 2.7

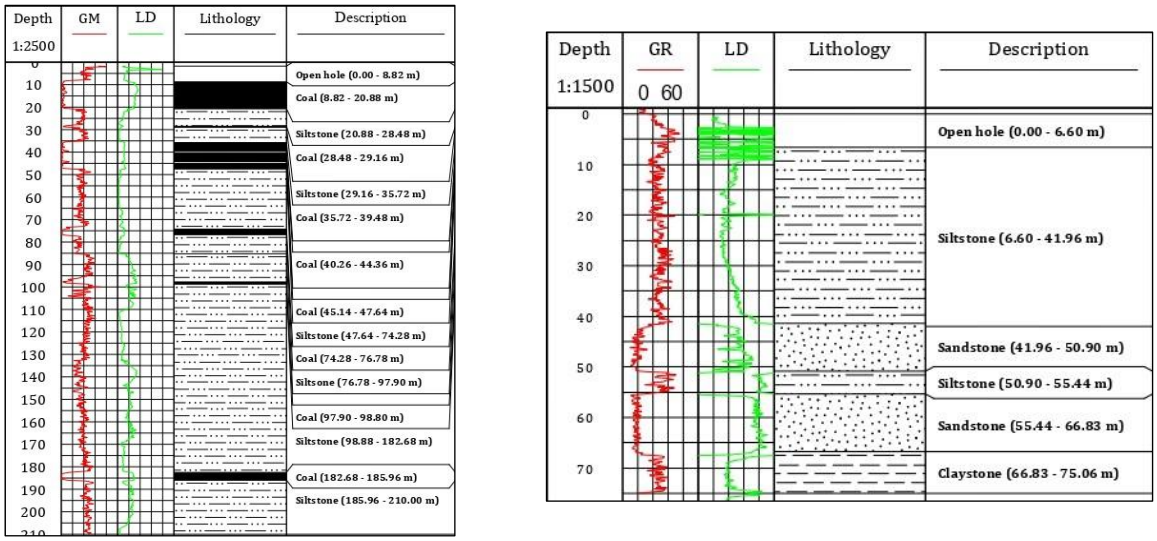
To strengthen the interpretation of reflection patterns in the radargram, an analysis of the characteristics of several rock types was conducted using gamma-ray and density logs, as presented in Table 2. Based on these rock log characteristic references, interpretation results were obtained from 4 borehole log points to identify subsurface lithology, as displayed in Figures 4a, 4b, 4c, and 4d.



(a)



(b)



(c) (d)

Figure 4. Borehole log processing interpretation at point BV_A (a), point BV_B (b), point BV_C (c), and point BV_D (d)

From the borehole log processing results at all four points, the coal layers exhibit low gamma-ray log responses and low-density log responses. The low gamma-ray values in coal are due to the very low content of radioactive elements, as coal is predominantly composed of carbon. Meanwhile, the low-density log response is attributed to coal's relatively low density, which results from its high porosity. Based on these response characteristics, the presence of coal seams indicates considerable variation in depth, as shown in Table 3.

Table 3. Coal seams intervals identified from borehole log interpretation

Borehole Point	Coal Seams Interval (m)	Thickness (m)
BV_A	82.02 – 95.80	13.78
	96.61 – 97.37	0.76
BV_B	46.05 – 49.61	3.56
BV_C	8.82 – 20.88	12.06
	28.48 – 29.16	0.68
	35.72 – 39.48	3.76
	40.26 – 44.36	4.10
	45.14 – 47.64	2.5
	74.28 – 76.78	2.5
	97.9 – 98.8	0.9
	182.68 – 185.96	3.28

In contrast to the three aforementioned points, no coal layers were identified at point BV_D, as indicated by the dominance of siltstone, sandstone, and claystone lithologies. The borehole log data were subsequently correlated with the GPR interpretation to identify the location and continuity of coal-bearing zones. However, coal occurrences at depths greater than 60 m were interpreted solely from borehole logging data and were not directly correlated with the 25 MHz GPR radargram. This is because the interval exceeds the penetration depth of the GPR data. Therefore, lithological information at these depths is derived exclusively from borehole log data.

The correlation between boreholes and GPR data is carried out by projecting the borehole positions onto the GPR survey line based on their coordinates, so that the location of each borehole along the survey line can be determined. The closer a borehole is to the survey line, typically within about 10–15 m, the higher the confidence level of the correlation. Before comparison, the seam depth

from the borehole logging data is corrected for elevation differences between the borehole and the survey line. Reflectors are then identified as coal seams based on the match in depth with the logging data and the presence of high-amplitude reflection characteristics indicating coal. Validation is further strengthened using outcrop data, allowing the reflectors observed on the radargram to be correlated with the same coal seam.

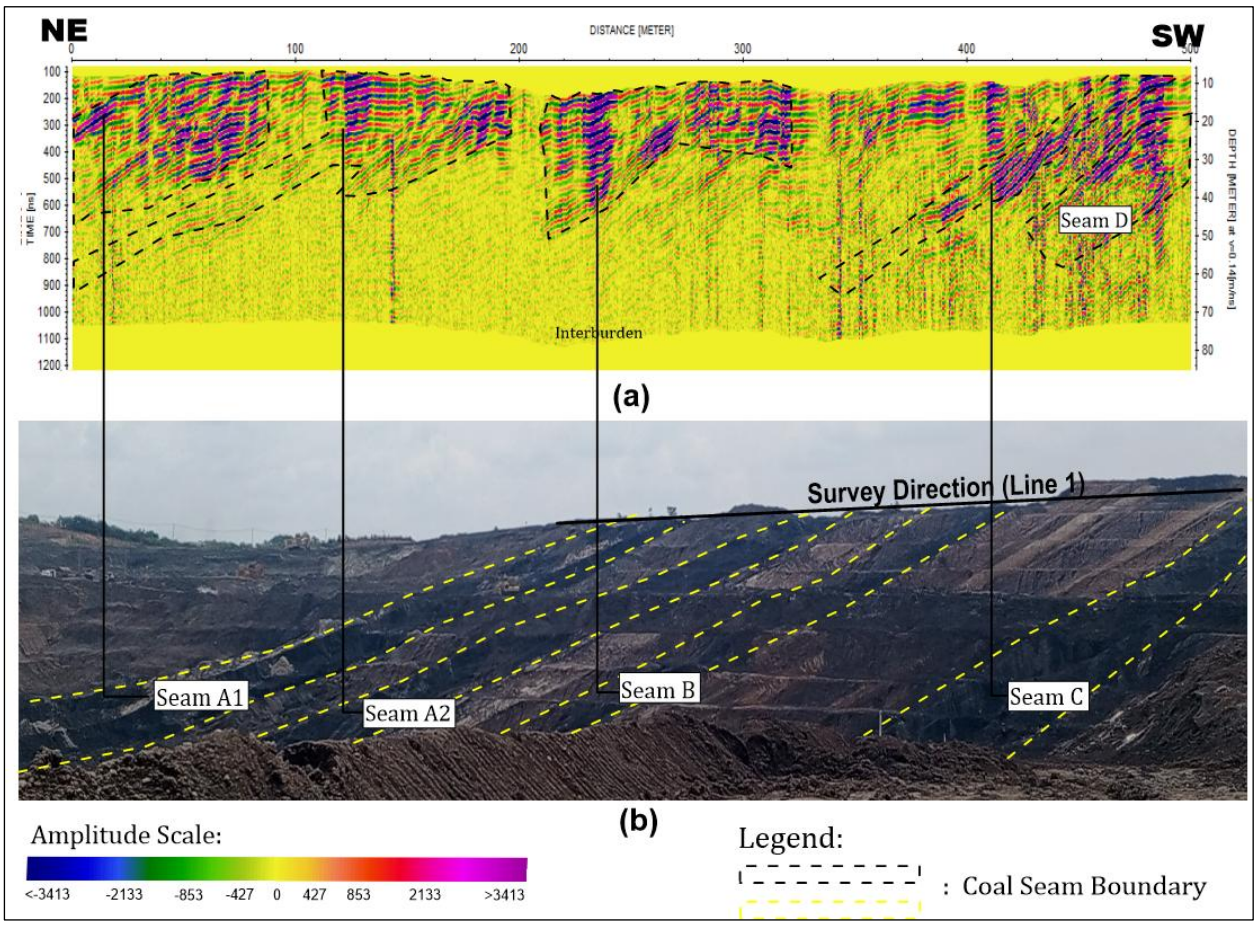


Figure 5. Interpretation of line 1 (a) and correlation with field outcrops (b)

Based on the radargram interpretation results for line 1, five main coal horizons were identified and correlated as Seam A1, A2, B, C, and D. Seam A1 appears as a high-amplitude reflector that can be traced over a distance of approximately 5–120 m, with depths ranging from 8–30 m. Beneath it, Seam A2 was identified at a distance of approximately 130–210 m and a depth of about 10–30 m. Seam B appears at a distance of approximately 240–320 m at depths of about 8–40 m, while Seam C is located at a distance of approximately 410–460 m with depths of about 8–45 m. Seam D is the deepest reflector observed, occurring at a distance of approximately 460–490 m and depths ranging from about 30–55 m. Although the reflectors show a dipping tendency on the radargram, the depth variations of each seam are relatively small along the survey line. This condition is thought to result from the survey line orientation being opposite to, or forming a large angle with, the continuity direction of the coal seams.

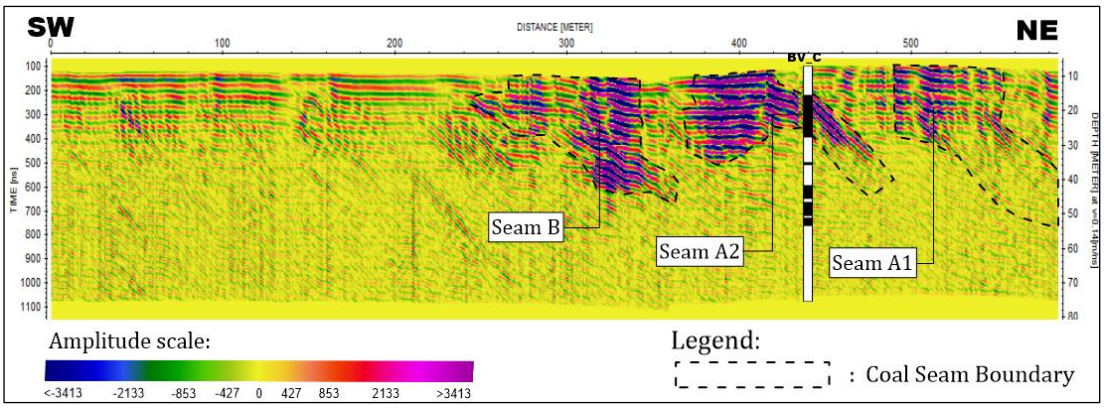


Figure 6. Radargram interpretation results and borehole log data correlation on line 2

Figure 6 shows line 2 oriented in the Southwest–Northeast direction. the reflector correlated as Seam A1 was identified at a distance of approximately 480–550 m with a depth of about 8–28 m. Seam A2 appears at a distance of 360–470 m with a depth of approximately 10–35 m, while Seam B was identified at a distance of around 250–340 m with depths ranging from 15–45 m. All three seams exhibit strong reflection characteristics and have fairly good lateral continuity. The relatively small depth variations in each seam indicate that the survey line does not follow the main dip direction of the coal layers. If the line were parallel to the dip direction, the depth difference between the two ends of the line would be much greater. Instead, because the line intersects the continuity of the layers, the seam positions on the radargram tend to remain within a nearly constant depth range. This condition is also supported by the correlation with borehole BV_C data, which shows that the coal seams occur at depth intervals that do not differ significantly from those interpreted from the radargram.

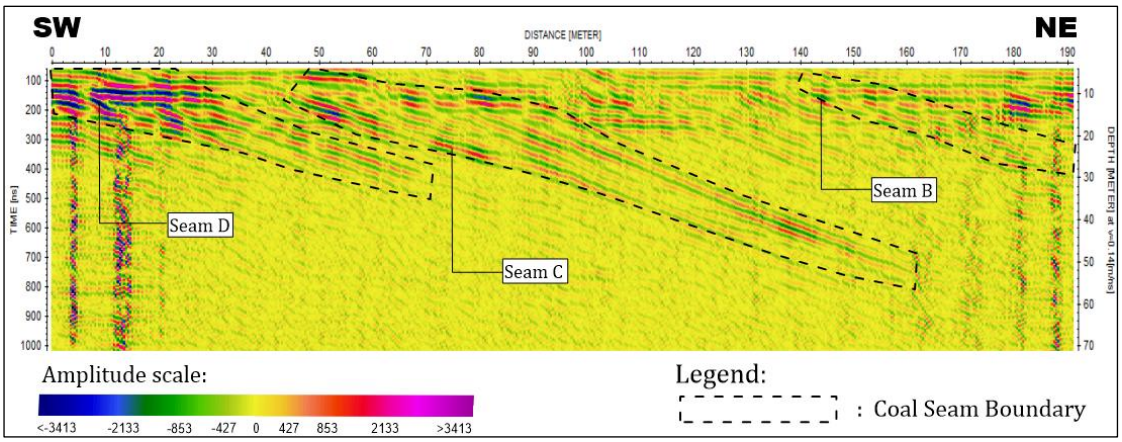


Figure 7. Radargram interpretation display several coal layers on line 3A

Figure 7 shows line 3A oriented in the Southwest–Northeast direction. The radargram interpretation results on Traverse 3A indicate the presence of three coal layers identified as Seam D, Seam C, and Seam B. This interpretation is based on the appearance of relatively high-amplitude reflectors that form parallel patterns and can be traced laterally along the traverse. Seam D is identified at a distance of approximately 0–65 m with a depth of 10–35 m, while Seam C is located at a distance of 70–140 m with a depth of 15–50 m. Seam B appears in the northeastern part of the traverse at a distance of 145–190 m with a depth of approximately 15–30 m. The coal layers are indicated by reflector patterns that are more regular and have stronger reflection energy compared to the interburden layers between them. This pattern suggests that the coal layers in the Traverse 3A area have fairly good continuity and still maintain a consistent stratigraphic position. The three seams are separated by interburden layers characterized by weaker amplitudes and less continuous reflection patterns.

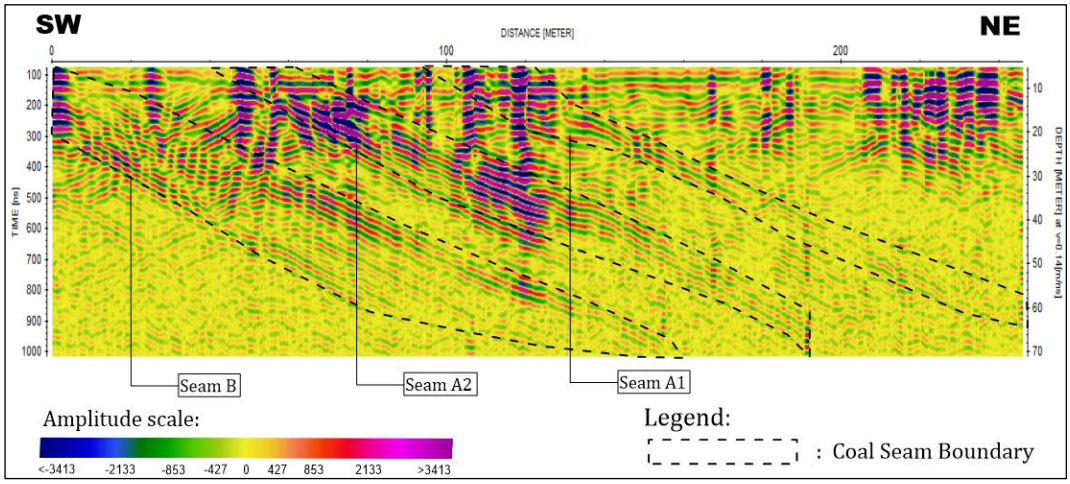


Figure 8. Radargram interpretation showing the coal seams with the high amplitude on line 3B

Figure 8 shows the processing results of line 3B with a Southwest–Northeast measurement direction. The radargram three coal layers were identified, namely Seam A1, Seam A2, and Seam B. Seam A1 and A2 appear to form closely spaced reflectors separated by a weaker non-coal layer, indicating seam splitting. In the lower part of the radargram, Seam B was also identified at a greater depth. The clarity of the A1 and A2 reflectors serves as the primary indicator of coal presence because they exhibit a striking amplitude contrast compared to the layers above and below them. In addition, the reflector shapes remain recognizable throughout the traverse, indicating that both seams have a relatively wide lateral extent. Furthermore, the interpretation of Traverse 3B is strengthened by its position, which is relatively parallel to Traverse 3A. The similar orientation of the two traverses allows lateral correlation between the reflectors appearing on each radargram. The presence of Seam B identified on both traverses indicates that this layer has fairly good continuity across the study area. Although Seams A1 and A2 are more dominant on Traverse 3B, while Seams C and D are more clearly observed on Traverse 3A, this difference is likely due to the positions of the two traverses intersecting different stratigraphic sections of the same coal-bearing system. Similar reflection characteristics, including relatively high amplitudes, continuous reflector patterns, and consistent stratigraphic positions, indicate that the coal layers in the study area are well developed laterally.

The quality of GPR signals can decrease due to attenuation in clay layers, water-saturated zones, and high-conductivity materials, causing reflectors at greater depths to become less distinct. In addition, the relatively low resolution of a 25 MHz antenna may limit the identification of thin seams, while survey line orientations that are not perpendicular to the layers can produce apparent dip. These results are consistent with previous coal GPR studies, which indicate that low frequencies are effective for mapping deep seams but have resolution limitations and are sensitive to subsurface geological conditions. Based on the survey line map, the GPR line direction extends from southwest to northeast, while the continuity of coal layers in the field is not aligned with these lines but instead runs in a different, oblique direction. This condition influences the resulting radargram responses. Survey lines that are not parallel to the strike direction of the coal layers cause reflectors to appear truncated and with limited continuity on the cross-section.

4. CONCLUSION

The GPR method with a frequency of 25 MHz is capable of identifying coal seams in PIT "SWIM", South Palembang Sub-Basin, through high-amplitude and relatively continuous reflectors that represent the contrast in dielectric constants between coal and the surrounding rocks within the Muara Enim Formation. The interpretation results, correlated with borehole log data, identified five coal seams at depths of 8–60 meters, namely seams A1, A2, B, C, and D. Although differences in survey line orientation relative to layer continuity caused dipping features on the radargrams, interpretation could still be carried out effectively through the integration of GPR data, borehole logs, and field observations. Practically, GPR has the potential to be an efficient method for shallow coal

exploration, and future studies are recommended to use survey lines parallel to the strike of the layers and integrate other geophysical methods to improve interpretation accuracy. This study also illustrates the practical application of electromagnetic wave physics principles, such as reflection coefficients, attenuation, and skin depth, in subsurface exploration, making it relevant as an example of applied physics learning that connects theoretical concepts with geophysical instruments.

REFERENCES

Adrian, D., & Mulyatno, B. S. (2020). Identifikasi dan Estimasi Sumber Daya Batubara Menggunakan Metode Poligon Berdasarkan Interpretasi Data Logging pada Lapangan "ADA", Sumatera Selatan. *JGE (Jurnal Geofisika Eksploras), 4*(1), 73-87. https://doi.org/10.23960/jge.v4i1.8

Alifa, F. (2024). *Interpretasi dan Korelasi Data Well Logging dalam Penentuan Volume dan Kualitas Batubara Berdasarkan Analisis Proksimat pada Daerah Tambang Air Laya PT. Bukit Asam Tbk., Tanjung Enim, Sumatera Selatan.* Lampung University, Department of Geophysical Engineering, Faculty of Engineering. Digital Repository UNILA.

Anwar, A. R., Abdurrokhim, Firmansyah, Y., & Gani, R. M. (2021). Fasies dan Lingkungan Pengendapan Batubara Formasi Muara Enim Lapangan "BIMA", Daerah Lubuk Betung, Sumatera Selatan. *Padjadjaran Geoscience Journal, 5*(6), 592-597. https://doi.org/10.24198/pgj.v5i6.38389

Balanis, C. A. (2012). *Advanced Engineering Electromagnetics (2nd ed.).* (J. W. Sons, Ed.)

Barber, A. J., Crow, M. J., & Milsom, J. S. (2005). *Sumatra: Geology, Resources and Tectonic Evolution* (Vol. Memoir 31). Geological Society of London.

Daniels, D. J. (2004). *Ground Penetrating Radar (2nd ed.).* London: The Institution of Engineering and Technology (IET). https://doi.org/10.1049/PBRA015E

Elfarabi, Widodo, A., & Syaifudin, F. (2017). Pengolahan Data Ground Penetrating Radar (GPR) dengan Menggunakan Software MATGPR R-3.5. *Jurnal Teknik ITS, 6*(1), 48-50.

Fang, L., Yang, F., Xu, M., & Liu, F. (2023). Research on Development 3D Ground Penetrating Radar Acquisition and Control Technology for Road Underground Diseases with Dual-Band Antenna Arrays. *MDPI Sensors, 23*(19), 1-14. https://doi.org/10.3390/s23198301

Farahdila, S., & Setiawan, B. (2023). Pemodelan Sebaran Ketebalan Batubara dan Sumberdata Batubara pada Tambang SBJ di PT. Bukit Asam Tanjung Enim, Sumatera Selatan. *Jurnal Penelitian Sains, 25*(3), 233-241. https://doi.org/10.56064/jps.v25i3.866

Feng, D., Liu, Y., Zhang, B., & Wang, X. (2023). Special Issue on Ground Penetrating Radar: Theory, Methods, and Applications. *Applied Sciences (Switzerland), 12*(17), 10-12. https://doi.org/10.3390/app13179847

Francke, J., & Utsi, V. (2009). Advances in Long-Range GPR Systems and Their Applications to Mineral Exploration, Geotechnical and Static Correction Problems. *IDS Ingegneria Dei Sistemi S.p.A, 27*(7). https://doi.org/10.3997/1365-2397.27.1301.29031

Geo, G. (2023). *MALÅ GroundVision 2.* https://www.guidelinegeo.com/products/mala-groundvision/

Ibrahim, E., Basri, H., & Alam, I. S. (2007). Penggunaan Metode GPR dan Geolistrik pada Eksplorasi Batubara. *Seminar Nasional Teknologi Industri XIII*, (pp. 1-8).

Jol, H. M. (2009). *Ground Penetrating Radar: Theory and Applications.* Cardiovascular Imaging. http://www.lavoisier.fr/notice/fr283071.html

Jovanovski, G., Boev, B., & Makreski, P. (2023). Chemistry and Geology of Coal: Nature, Composition, Coking, Gasification, Liquefaction, Production of Chemicals, Formation, Peatification, Coalification, Coal Types, and Ranks. *Springer Nature Link, 9*(2), 1-16. https://doi.org/10.1007/s40828-022-00177-y

Jufri, N., Lantu, & Massinai, M. A. (2015). *Aplikasi Metode Ground Penetrating Radar (GPR) Untuk Identifikasi Seam Batubara.* Universitas Hasanuddin, Program Studi Geofisika, Jurusan Fisika, Fakultas Matematika dan Ilmu Pengetahuan Ala,, Makassar.

Marbun, M. C., Supriyanto, & Rinald, A. (2020). Identifikasi Lapisan Penyebab Longsor Menggunakan Ground Penetrating Radar Area Monumen Pesawat Sangatta (PT. Kaltim Prima Coal). *Jurnal Geosains Kutai Basin Vomue, 3*(2). https://doi.org/10.30872/geofisunmul.v3i2.692

Maulana, R., Dewanto, O., & Abriansyah, R. (2020). Karakterisasi Lapisan Batubara Pada Tambang Arantiga Dan Seluang Bengkulu Menggunakan Analisis Data Proksimat. *JGE (Jurnal Geofisika Eksplorasi), 6*(3), 197-204. https://doi.org/10.23960/jge.v6i3.92

Ministry of Energy and Mineral Resources. (2021). *Road Map Pengembangan dan Pemanfaatan Batubara (Grand Strategy Hilirisasi Batubara).* Ministry of Energy and Mineral Resources. https://www.esdm.go.id/assets/media/content/content-buku-road-map-pengembangan-dan-pemanfaatan-batubara.pdf

Mowrey, G. L. (1991). Promising Coal Interface Detection Methods. *Mining Engineering (Society for Mining, Metallurgy & Exploration – SME), 43*(1), 134–138. https://doi.org/10.1016/0148-9062%2891%2990838-d

Murray, W., Lewis, C., Yang, Z., & Pollock, J. T. (1996). Development of High Resolution GPR Hardware in the Frequency Range 300 MHz–3.5 GHz. *Proceedings of the 6th International Conference on Ground Penetrating Radar (GPR 96)*, (pp. 505–510).

Neal, A. (2004). Ground Penetrating Radar and Its Use in Sedimentology: Principles, Problems, and Progress. *Earth-Science Reviews, 66*(3-4), 261-330. https://doi.org/10.1016/j.earscirev.2004.01.004

Nursanto, E., Haq, S. R., & Ardian, A. (2023). Karakteristik Batubara Formasi Warukin di Kalimantan Selatan serta Implikasinya pada Teknologi Pencairan Batubara. *Jurnal Mineral, Energi, dan Lingkungan, 7*(2), 51-57. https://doi.org/10.31315/jmel.v7i2.11075

Priyanka, P., Ashutosh, A. D., Neha, S. R., & Maske, M. M. (2022). Review of Applications of Ground Penetrating Radar as an NDT Tool. *ASEAN Journal of Science and Engineering, 2*(1), 115-128. https://doi.org/10.17509/ajse.v2i2.37975

Ralston, J. C., & Hainsworth, D. W. (1999). Application of Ground Penetrating Radar for Coal Depth Measurement. *IEEE International Conference on Acoustics, Speech, and Signal Processing (ICASSP), 4*, 2275–2278. https://doi.org/10.1109/ICASSP.1999.758391

Ralston, J. C., & Hainsworth, D. W. (2000). Use of Ground Penetrating Radar in Underground Coal Mining. *Proceedings of SPIE – The International Society for Optical Engineering, 4084*, 731–742. https://doi.org/10.1117/12.383507

Ramadhana, I., Mardiana, U., Muljana, B., & Irvan, H. M. (2022). Fasies pengendapan Batubara Formasi Muara Enim di Tambang Air Laya, Cekungan Sumatra Selatan. *Padjajaran Geoscience Journal, 6*(4), 994-1006. https://doi.org/10.24198/pgj.v6i4.45245

Rumansah, R. P., Paembonan, A. Y., & Andika, P. P. (2025). Pengembangan Aplikasi "ITERA-VISION-GPR-UI (ITERA Vision System GPR Utilities Inference)" Berbasis Computer Vision dengan Model YOLOv12 untuk Deteksi Utilitas pada Metode Ground Penetrating Radar. *Journal Online of Physics, 11*(1), 120-131. https://doi.org/10.22437/jop.v11i1.49883

Sandmeier, K. J. (2020). Main news of the REFLEXW version 9.5a.

South Sumatra Provincial Government. (2025). *Rencana Pembangunan Jangka Menengah Daerah Provinsi Sumatera Selatan.* South Sumatra Provincial Government.

Strange, A. D., & Jecny, Z. (2020). Development of Digital Subterranean Models for Real-Time Open Cut Horizon Control. *International Journal of Mining Science, 9*(4), 1-17. https://doi.org/10.3390/resources9040050

Syukri, M. (2020). *Pengantar Geofisika.* Syah Kuala University Press.

Tian, Y., Li, C., Wang, Z., Chen, S., Lyu, F., Zhang, Q., & Hu, D. (2025). Method for Ground Penetrating Radar Identification of Intercalated Gangue Layers during Complex Structure Coal Seam Tunneling. *Journal of Electromagnetic Engineering and Science, 25*(3), 222-230. https://doi.org/10.26866/jees.2025.3.r.292

Unver, B. (2018). Fundamentals of 3D Modelling and Resource Estimation in Coal Mining. *Journal of Mining & Environment, 9*(3), 623-639. https://doi.org/10.22044/jme.2018.6848.1515